

# Collisional spin transfer in an atomic heteronuclear spinor Bose gas

Fang Fang,<sup>1,\*</sup> Joshua A. Isaacs,<sup>1</sup> Aaron Smull,<sup>1</sup> Katinka Horn,<sup>1,†</sup> L. Dalila Robledo-De Basabe,<sup>1</sup> Yimeng Wang,<sup>2</sup> Chris H. Greene,<sup>2,3</sup> and Dan M. Stamper-Kurn<sup>1,4</sup>

<sup>1</sup>Department of Physics, University of California, Berkeley, California 94720, USA

<sup>2</sup>Department of Physics and Astronomy, Purdue University, West Lafayette, Indiana 47907, USA

<sup>3</sup>Purdue Quantum Science and Engineering Institute,

Purdue University, West Lafayette, Indiana 47907, USA

<sup>4</sup>Materials Sciences Division, Lawrence Berkeley National Laboratory, Berkeley, California 94720, USA

We observe spin transfer within a non-degenerate heteronuclear spinor atomic gas comprised of a small <sup>7</sup>Li population admixed with a <sup>87</sup>Rb bath, with both elements in their  $F = 1$  hyperfine spin manifolds and at temperatures of 10's of  $\mu\text{K}$ . Prepared in a non-equilibrium initial state, the <sup>7</sup>Li spin distribution evolves through incoherent spin-changing collisions toward a steady-state distribution. We identify and measure the cross-sections of all three types of spin-dependent heteronuclear collisions, namely the spin-exchange, spin-mixing, and quadrupole-exchange interactions, and find agreement with predictions of heteronuclear <sup>7</sup>Li-<sup>87</sup>Rb interactions at low energy. Moreover, we observe that the steady state of the <sup>7</sup>Li spinor gas can be controlled by varying the composition of the <sup>87</sup>Rb spin bath with which it interacts.

The spin dynamics of a gas of itinerant particles are central to a range of phenomena in atomic and condensed-matter physics. In solid state, spin relaxation governs the penetration depth of non-equilibrium electron spin distributions injected from ferromagnetic into non-magnetic materials [1, 2], affecting spintronics and their applications in magnetic data storage and sensing. The spin-dependent exchange interaction leads to diffusive spin waves in atomic Bose [3, 4] and Fermi gases [5] and in electronic systems [6]. Spin relaxation collisions also determine the rate of demagnetization cooling of atomic gases [7–10].

The trapping of atomic gases within spin-independent optical traps enables the study of spinor Bose and Fermi gases, in which atoms may populate any of the magnetic sublevels within a manifold of fixed total atomic spin [11]. These gases present a controlled medium for the study of magnetic ordering, phase transitions, and non-equilibrium spin dynamics. Recently, such studies have extended to heteronuclear spinor gases, comprised of spinor gases of two different elements or isotopes [12].

Like the homonuclear spinor gas, the heteronuclear system evolves through spin-dependent interactions that preserve rotational symmetry. Neglecting effects of magnetic dipole-dipole interactions, heteronuclear s-wave collisions preserve the total spin projection of the colliding atom pair along a chosen quantization axis (defined as  $\mathbf{z}$ ). Labeling the state of a <sup>7</sup>Li-<sup>87</sup>Rb atom pair, with both atoms in the  $F = 1$  atomic spin manifold, by the magnetic quantum numbers  $m_z$  of the two atoms, we identify three distinct processes that transfer spin between the two spinor gases (Fig. 1): spin exchange (exemplified by the process  $|0_{\text{Li}}, -1_{\text{Rb}}\rangle \leftrightarrow |-1_{\text{Li}}, 0_{\text{Rb}}\rangle$ ) and spin mixing (e.g.  $| -1_{\text{Li}}, +1_{\text{Rb}}\rangle \leftrightarrow |0_{\text{Li}}, 0_{\text{Rb}}\rangle$ ), both of which transfer one quantum of spin between the spinor gases; and quadrupole exchange (e.g.  $| +1_{\text{Li}}, -1_{\text{Rb}}\rangle \leftrightarrow |-1_{\text{Li}}, +1_{\text{Rb}}\rangle$ ), which transfers two spin quanta. Experi-

ments to date have focused only on spin exchange within <sup>23</sup>Na-<sup>87</sup>Rb [12] and <sup>7</sup>Li-<sup>23</sup>Na [13] heteronuclear spinor gases.

In this work, we characterize spin relaxation in the heteronuclear <sup>7</sup>Li-<sup>87</sup>Rb spinor gas. We prepare non-degenerate gas mixtures with a large number imbalance, so that the majority population of Rb atoms serves as a spin bath of near-constant Zeeman-state distribution, and then observe how the minority population of Li atoms evolves through incoherent spin-changing collisions with this bath. To make an analogy with spintronics, the Rb bath plays the role of a magnetic material and the Li atoms play the role of an injected non-equilibrium electron current. By comparing spin relaxation from several initial states, we identify and characterize the strength of each of these spin-changing processes. This approach allows us, for the first time, to obtain a complete experimental characterization of spin-dependent interactions in a heteronuclear spinor gas.

Li-Rb gas mixtures are prepared in a two-species compressed magneto-optical trap (MOT) [14]. During the last 0.5 s of loading this MOT, an optical dipole trap is introduced, formed by a single beam of light of 1060-nm wavelength, and focused to a  $1/e^2$  beam radius of 34  $\mu\text{m}$  at the MOT center. This optical trap has trap depth of  $k_B \times 330 \mu\text{K}$  and frequencies  $\omega_{x,y,z} = 2\pi \times (5700, 5700, 34) \text{ s}^{-1}$  for Li, and of  $k_B \times 840 \mu\text{K}$  and  $\omega_{x,y,z} = 2\pi \times (2600, 2600, 16) \text{ s}^{-1}$  for Rb. After the MOT is turned off, a final stage of optical cooling leaves an optically trapped gas of about  $2 \times 10^5$  <sup>7</sup>Li atoms at a temperature of  $T_{\text{Li}} = 36 \mu\text{K}$ , and about  $2 \times 10^6$  <sup>87</sup>Rb atoms at a temperature of  $T_{\text{Rb}} = 87 \mu\text{K}$ . Since the ratio of the temperature to the trap depth are similar for the two elements, they occupy the same volume within the trap. Differential effects of gravity (oriented along  $\mathbf{y}$ ) are negligible.

The two spinor gases are initially unpolarized, with

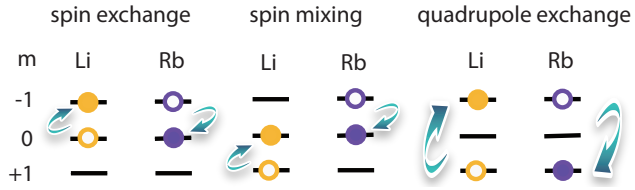


FIG. 1. A heteronuclear spinor gas, with both spinor gases in their respective  $F = 1$  spin manifolds, undergoes three distinct types of spin-changing s-wave collisions: spin exchange, spin mixing, and quadrupole exchange. One possible channel is shown for each collision, with initial and final Zeeman states indicated by an open and a closed symbol, respectively. We assume spinor-gas collisions respect rotational symmetry and ignore effects of magnetic dipole-dipole interactions.

equal population in all three magnetic sublevels of the  $F = 1$  spin manifolds and no transverse coherence between sublevels. To initiate spin dynamics, we polarize the gas through element-selective optical pumping on either the D1 (Li) or D2 (Rb) principal atomic resonances. Pumping with either  $\sigma_+$  or  $\sigma_-$  polarized light propagating in the direction of an applied magnetic field, we drive either element selectively into the  $|m_F = +1\rangle$  or  $|m_F = -1\rangle$  states, respectively, with final state fidelity of nearly 100% for Li and around 80% for Rb. A wider range of initial states can be accessed by applying rf magnetic field pulses resonant with the Larmor frequency. For example, by optically pumping the Rb gas, applying a resonant rf pulse with pulse angle  $\phi$ , and then optically pumping the Li gas, we prepare the initial spin configuration shown in Fig. 2(a), with Li occupying the  $|m_F = -1\rangle$  state and the Rb bath occupying a variable mixture of magnetic sublevels.

The atoms are allowed to evolve for a variable time of several seconds before the spin composition of each gas is measured. We measure the total  $N_{m_F}^{(Rb)}$  and fractional  $p_{m_F}^{(Rb)}$  Rb populations in each magnetic sublevel using state-selective absorption imaging [15, 16]. In this method, a weak microwave-frequency pulse excites Rb atoms from a selected  $F = 1$  sublevel into the  $F = 2$  manifold, after which the  $F = 2$  population is quantified *in-situ* through resonant absorption imaging [17].

We quantify the Li spin distribution differently. Prior to imaging, we impose a spherical quadrupole magnetic field (with axis along  $\mathbf{y}$ ) atop the optical trap [18]. At a low magnetic field gradient ( $B'_y = 58$  G/cm), magnetic forces expel all lithium atoms in the  $|m_F = +1\rangle$  sublevel, but allow atoms in the remaining sublevels to remain trapped. At a higher gradient ( $B'_y = 270$  G/cm) the quadratic Zeeman shift is sufficiently strong that the  $m_F = 0$  atoms are also expelled, leaving only the weak-field seeking  $m_F = -1$  atoms. By counting the remaining trapped Li gas through spin-independent absorption imaging, we determine either the total atom number in

all sublevels  $N_{\text{tot}}^{(\text{Li})}$ , in both the  $|m_F = 0\rangle$  and  $|m_F = -1\rangle$  states  $N_{0,-1}^{(\text{Li})}$ , or in just the  $|m_F = -1\rangle$  state  $N_{-1}^{(\text{Li})}$ , depending on whether we had previously applied no gradient, a low gradient, or a high gradient, respectively.

In each repetition of the experiment, we make just one of the aforementioned measurements on just one of the two co-trapped elements. The full spin distribution is obtained by combining measurements from several repetitions of the same experimental sequence.

Our measurement results are presented in Fig. 2. An initially spin polarized Li gas undergoes spin relaxation over the course of several seconds, and both the nature and final state of this relaxation varies as the spin polarization of the co-trapped Rb spin bath is varied. We present several arguments for why the lithium spin distribution evolves solely due to spin-dependent Li-Rb collisions. First, we conducted separate experiments in which a single-species gas of either Li or Rb was found to remain spin polarized in the optical trap, demonstrating that spin relaxation is not caused by external factors such as magnetic field noise or light scattering. Second, we may discount the effect of spin-changing Li-Li collisions, relative to that of Li-Rb collisions, given that the Rb atom number is much larger than the Li atom number. Third, we may neglect spin-changing Rb-Rb collisions over the measurement duration because the rate of spin-mixing collisions in  $^{87}\text{Rb}$   $F = 1$  spinor gases is anomalously small [19].

We compare the observed spin relaxation to a model for spin-dependent interactions in a heteronuclear spinor gas. We distinguish between the spin-dependent effects of forward scattering, in which the momenta of the colliding particles do not change in a collision, and non-forward scattering, in which they do. Forward scattering leads to collective mean-field effects such as Zeeman-state-dependent energy shifts and to dynamics where spin is coherently transferred between the two spinor gases. These coherent dynamics, which have been observed in quantum-degenerate heteronuclear spinor gases [12, 13], are driven by transverse coherence between Zeeman populations. In our system, however, such transverse coherence is found to be damped rapidly, within just a few ms, owing to magnetic field inhomogeneity and atomic motion [20]. Such damping suppresses coherent collisional spin transfer.

Non-forward scattering, in a non-degenerate gas, leads only to incoherent transfer of spin between spinor gases. Considering a uniform mixture of spinor gases  $A$  and  $B$ , the per-atom rate at which atoms in gas  $A$  and sublevel  $m_A$  undergo a spin-changing collision is given as  $\Gamma_\alpha p_{m_B}^{(B)} = n^{(B)} \bar{v} \sigma_\alpha p_{m_B}^{(B)}$  where  $n^{(B)}$  is the density of gas  $B$  atoms,  $\bar{v}$  is the rms incident velocity,  $\sigma_\alpha$  is the cross section, and  $p_{m_B}^{(B)}$  is the fraction of gas  $B$  atoms in the incident spin state for the specific spin-changing collision considered (labeled by  $\alpha$ ) [21].

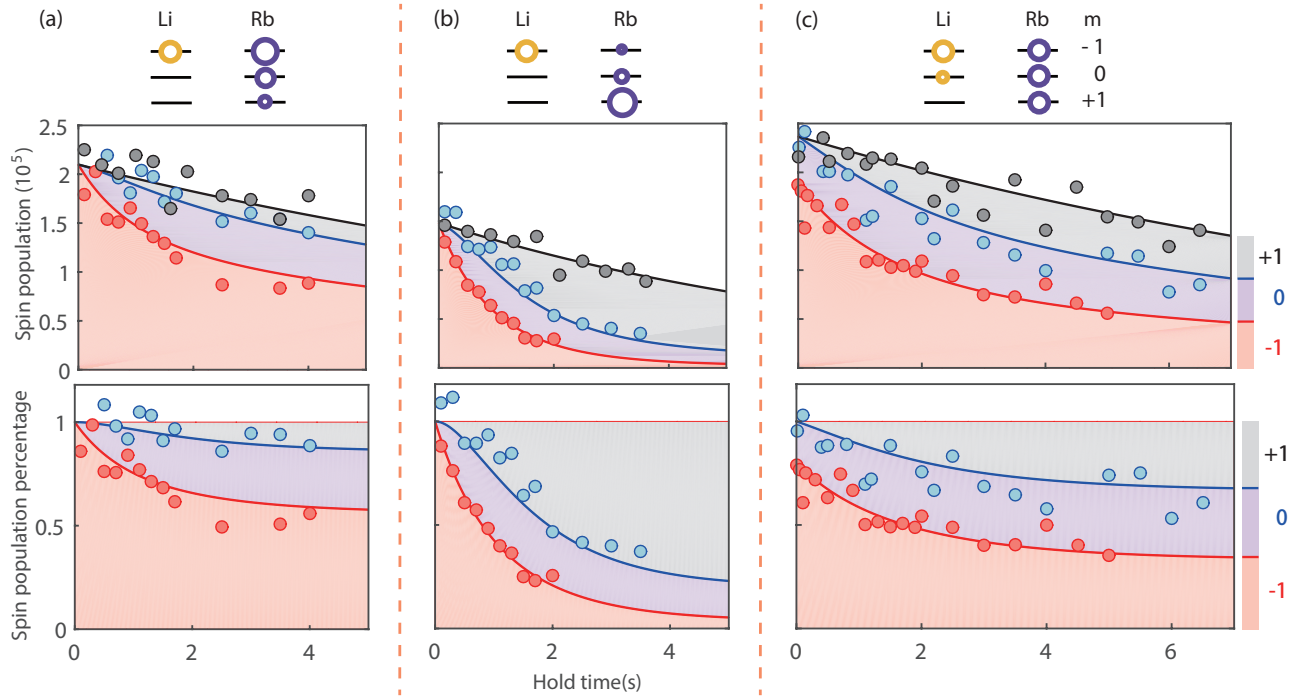


FIG. 2. Spin relaxation of a  ${}^7\text{Li}$  gas in the presence of a  ${}^{87}\text{Rb}$  spin bath. Top row: The Li and Rb gases are prepared in one of three initial spin configurations (a-c), with Zeeman-state distributions indicated graphically. Measurements of  $N_{-1}^{(\text{Li})}$  (red),  $N_{0,-1}^{(\text{Li})}$  (blue) and  $N_{\text{tot}}^{(\text{Li})}$  (gray) and the corresponding fractional populations are shown in the middle and bottom row, respectively. Data are overlaid with results of a fit of all measurements to the rate-equation model (Eq. 1). Shaded areas indicate the Li populations in the  $m_F = -1$  (red), 0 (purple), and +1 (gray) sublevels. The Rb atom number of  $2 \times 10^6$  in scheme (b) is somewhat larger than the  $1.6 \times 10^6$  Rb atom number for schemes (a) and (c).

Following these considerations, we describe the evolution of spin populations in our Li gas,  $\mathbf{N}^{(\text{Li})} =$

$\left( N_{+1}^{(\text{Li})}, N_0^{(\text{Li})}, N_{-1}^{(\text{Li})} \right)^\top$  through the rate equation

$$\frac{d\mathbf{N}^{(\text{Li})}}{dt} = -\frac{\mathbf{N}^{(\text{Li})}}{\tau} + \begin{pmatrix} -\Gamma_{\text{se}} p_0 - (\Gamma_{\text{sm}} + \Gamma_{\text{qe}}) p_{-1} & \Gamma_{\text{se}} p_{+1} + \Gamma_{\text{sm}} p_0 & \Gamma_{\text{qe}} p_{+1} \\ \Gamma_{\text{se}} p_0 + \Gamma_{\text{sm}} p_{-1} & -\Gamma_{\text{se}} (p_{+1} + p_{-1}) - 2\Gamma_{\text{sm}} p_0 & \Gamma_{\text{se}} p_0 + \Gamma_{\text{sm}} p_{+1} \\ \Gamma_{\text{qe}} p_{-1} & \Gamma_{\text{se}} p_{-1} + \Gamma_{\text{sm}} p_0 & -\Gamma_{\text{se}} p_0 - (\Gamma_{\text{sm}} + \Gamma_{\text{qe}}) p_{+1} \end{pmatrix} \mathbf{N}^{(\text{Li})} \quad (1)$$

Here,  $\Gamma_{\text{se}}$ ,  $\Gamma_{\text{sm}}$  and  $\Gamma_{\text{qe}}$  quantify the rates of spin-exchange, spin-mixing, and quadrupole-exchange collisions, respectively. We make the simplifying assumption that the total atom number and Zeeman-state populations  $p_m^{(\text{Rb})} = p_m$  of the large Rb bath remain constant. We include also an overall, spin-independent loss term with trap lifetime  $\tau$ , capturing the observation that Li atoms are lost preferentially from the optical dipole trap over the experiment duration.

Applying this rate-equation approach to our experimental situation neglects variations of the Li and Rb spin distributions in position, momentum and energy. We argue that these variations can be neglected owing to rapid atomic motion as compared to the slow Li-Rb collision

rates, and to the fact that non-forward scattering leads to effective redistribution of the Li-atom momentum.

Using Eq. 1, we apply a simultaneous least-squares fit to experimental observations in all three initial configurations shown in Fig. 2. In this fit, the cross-sections  $\sigma_{\text{se}}$ ,  $\sigma_{\text{sm}}$  and  $\sigma_{\text{qe}}$ , and also the initial total Li atom number at each experimental setting, are used as free parameters. The uniform Rb density in our expression for  $\Gamma_\alpha$  is replaced by the overlap density, which is around  $1.5 \times 10^{12} \text{ cm}^{-3}$ , determined based on measurements for each of the initial configurations. The relative velocity is calculated as a thermal average:  $\bar{v} =$

$$\sqrt{\frac{8k_B}{\pi} \left( \frac{T_{\text{Rb}}}{m_{\text{Rb}}} + \frac{T_{\text{Li}}}{m_{\text{Li}}} \right)} \simeq 0.36 \text{ m/s}, \text{ where } m_{\text{Rb}} \text{ and } m_{\text{Li}} \text{ are the atomic masses of Rb and Li, respectively.}$$

Quantity	Experiment	Theory
$\sigma_{\text{se}} (10^{-14} \text{ cm}^2)$	2.4(7)	2.2
$\sigma_{\text{sm}} (10^{-14} \text{ cm}^2)$	1.7(6)	1.8
$\sigma_{\text{qe}} \text{ (ub)} (10^{-14} \text{ cm}^2)$	0 <sup>(0.5)</sup> <sub>(0)</sub>	0.02
$\sigma_{\text{se}}/\sigma_{\text{sm}}$	1.4(6)	1.2
$ a_{\text{se}} (a_B)$	8.2(1.2)	7.8
$ a_{\text{sm}} (a_B)$	7.0(1.3)	7.2
$ a_{\text{qe}}  \text{ (ub)} (a_B)$	0 <sup>(3.8)</sup> <sub>(0)</sub>	0.7

TABLE I. Heteronuclear spin-dependent interaction strengths for the  ${}^7\text{Li}$ - ${}^{87}\text{Rb}$  spinor gas. Cross sections and effective scattering lengths obtained from experimental fits are compared to theoretical predictions. For experimental data, standard statistical errors, accounting for fitting errors and trap frequency, temperature, and Rb atom number measurements, are shown for the spin-exchange and spin-mixing processes, while standard upper (ub) and lower (lb) bounds are shown for the weaker quadrupole-exchange process.

We note that different initial conditions provide varying constraints on the measured cross-sections. For example, for initial conditions (a) (as indicated in Fig. 2), the observed spin relaxation of Li from the initial spin-polarized  $|m_F = -1\rangle$  state is dominated by the spin-exchange interaction, i.e. through collisions with the Rb  $m_F = 0$  population. Alternately, for initial condition (b), the  $|m_F = -1\rangle$  state of Li initially undergoes either spin-mixing or quadrupole-exchange interactions with the Rb bath that is mostly in the  $|m_F = +1\rangle$  state. The fact that we observe an immediate, linear growth of the Li population in the  $|m_F = 0\rangle$  state, followed more slowly by a rise in the  $|m_F = 1\rangle$  population, shows the spin-mixing process to dominate over the quadrupole-exchange process, i.e.  $\sigma_{\text{sm}} \gg \sigma_{\text{qe}}$ . The fact that spin relaxation from initial conditions (a) and (b) occurs at a comparable rate demonstrates that  $\sigma_{\text{se}}$  and  $\sigma_{\text{sm}}$  are comparable in value. The spin-dependent collision cross-sections determined from our fits, and shown in Table I, reflect these observations.

Low energy collisions between two spinor Bose gases are characterized fully by the s-wave scattering lengths  $a_{F_{\text{tot}}}$  labeled by the total angular momentum quantum number  $F_{\text{tot}}$  for the colliding atoms; here,  $F_{\text{tot}} \in \{0, 1, 2\}$ . Effective scattering lengths  $a_{\text{eff}}$  for the three allowed spin-changing collisions are calculated by considering the input and output spin states in the pair-spin basis. One finds  $a_{\text{se}} = (a_2 - a_1)/2$ ,  $a_{\text{sm}} = (a_2 - a_0)/3$  and  $a_{\text{qe}} = (a_2 - 3a_1 + 2a_0)/6$  for the spin-exchange, spin-mixing, and quadrupole-exchange processes, respectively. Collision cross sections for each process are calculated as  $\sigma = 4\pi a_{\text{eff}}^2$  [17].

We compute the scattering lengths  $a_{F_{\text{tot}}}$  through a coupled-channel scattering calculation that relies on the model of the  ${}^7\text{Li}$ - ${}^{87}\text{Rb}$  molecular potential characterized in Ref. [22]. Calculations are performed for a collision

energy of  $k_B \times 50 \mu\text{K}$ . As shown in Table I, our measurements of the spin-changing collision cross sections and effective scattering lengths are consistent with these predictions. We note that these effective scattering lengths  $a_{\text{eff}}$  are all obtained as differences between the scattering lengths  $a_{F_{\text{tot}}}$ , but do not determine their mean value. Previous measurements showed that this mean value differs from theoretical predictions at collision energies of 100's of  $\mu\text{K}$  [14]. We note also that our calculations predict the effective scattering lengths to be relatively independent of collision energy within the energy range probed in our present experiment.

Following several seconds of spin relaxation, the Li gas evolves to a spin-state distribution that depends on the spin composition of the Rb bath. This situation bears analogy to spintronic systems, where an electron current acquires magnetization after being injected into a ferromagnetic material. Assuming still that the Rb bath retains its initial spin-state distribution, this steady-state Li spin distribution is determined by the non-trivial zero-eigenvalue eigenvector of the matrix in Eq. 1.

Such steady-state distributions, determined from the measured spin-dependent cross sections, are presented in Fig. 3. Here, we characterize the spin distribution by its dimensionless longitudinal magnetization  $M_z = p_{+1} - p_{-1}$  and one component of the dimensionless quadrupole tensor  $Q_{zz} = \frac{1}{3} - p_0$ . While the full range of spin distributions is described by  $M_z$  ranging from -1 to +1 and  $Q_{zz}$  ranging from  $|M_z| - \frac{2}{3}$  to  $\frac{1}{3}$ , the full range of steady-state Li distributions, calculated for all possible distributions of the Rb bath, is predicted to occupy a narrow band of possible values. We test this prediction experimentally, considering the three Rb bath distributions shown in Fig. 2, and comparing the observed long-time Li distribution to that predicted theoretically, finding good agreement between the two.

Over much longer times, the spin distribution of the Rb gas should also evolve. Considering just the effects of Li-Rb collisions, the timescale for the evolution of the spin-state distribution of the Rb gas is longer than that of the Li gas by the factor  $N_{\text{tot}}^{(\text{Rb})}/N_{\text{tot}}^{(\text{Li})} \simeq 10$ . Over this long timescale, which was inaccessible in our experiment, the spin-state distributions of the two gases should acquire equal longitudinal magnetizations and quadrupole moments [17].

In conclusion, by characterizing spin relaxation in  ${}^7\text{Li}$ - ${}^{87}\text{Rb}$  gas mixtures, we have, to our knowledge, performed the first complete experimental determination of all spin-dependent interactions in a heteronuclear spinor gas. Our work highlights the richness of heteronuclear spinor gases. Whereas for homonuclear spinor gases the longitudinal magnetization is constant (neglecting magnetic dipole-dipole interactions) and determined manually, for the heteronuclear system, each spinor gas may undergo significant variation by exchanging magnetization with the other. Thus, by using one spinor gas as a large mag-

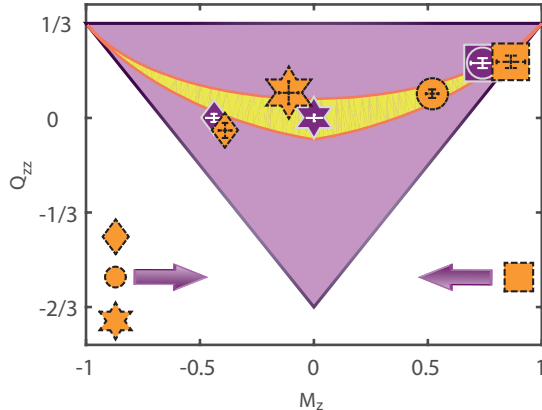


FIG. 3. Controlling the steady-state spin distribution of the  ${}^7\text{Li}$  spinor gas by varying the state of the  ${}^{87}\text{Rb}$  spin bath. Under conditions of zero transverse coherence, the  $F = 1$  spinor gas polarization is defined by the longitudinal magnetization  $M_z$  and quadrupole moment  $Q_{zz}$ , whose range is indicated by the purple shaded region. The  ${}^7\text{Li}$  steady state distribution is predicted to lie in a narrower region (shaded yellow) given all possible fixed polarizations of the  ${}^{87}\text{Rb}$  bath. Experimentally measured late-time  ${}^7\text{Li}$  distributions are marked by orange markers with dashed boundary, while the predicted distribution, based on measurements of the  ${}^{87}\text{Rb}$  gas spin distribution, are shown with purple markers. Four initial states are considered: (a) diamond, (b) circle, (c) star, and (Rb bath as in b, but Li initialized in  $|m_F = +1\rangle$  state) square. Here, the letters (a-c) refer to labels in Fig. 2.

netization reservoir, one may obtain a clearer picture of the thermodynamic behavior of the other spinor gas without artificial constraint. This work also points to a productive analogy between the dynamics of heteronuclear spinor gases and solid-state spintronics. For example, future work could study the evolution of an itinerant spinor gas, e.g. Li with its light mass, in the presence of another spatially localized spinor gas, e.g. a heavier gas such as Rb or Cs, in order to simulate the evolution of electrons within layered magnetic materials.

We acknowledge support from the National Science Foundation (PHY-1707756), DTRA (HDTRA1-15-1-0009), and by NASA-JPL (JPL1505588). KH acknowledges support by 'Hamburglobal', funded by the program 'Promos' of the German Academic Exchange Service (DAAD), issued through Universitt Hamburg. The work of CHG and YW has been supported by NSF grant PHY-1912350.

(1985).

- [3] N. P. Bigelow, J. H. Freed, and D. M. Lee, Phys. Rev. Lett. **63**, 1609 (1989).
- [4] J. McGuirk, H. Lewandowski, D. Harber, T. Nikuni, J. Williams, and E. Cornell, Phys. Rev. Lett. **89**, 090402 (2002).
- [5] X. Du, Y. Zhang, J. Petricka, and J. E. Thomas, Phys. Rev. Lett. **103**, 010401 (2009).
- [6] A. G. Aronov, Zhurnal Eksperimentalnoi I Teoreticheskoi Fiziki **73**, 577 (1977).
- [7] M. Fattori, T. Koch, S. Goetz, A. Griesmaier, S. Hensler, J. Stuhler, and T. Pfau, Nature Physics **2**, 765 (2006).
- [8] P. Medley, D. M. Weld, H. Miyake, D. E. Pritchard, and W. Ketterle, Phys. Rev. Lett. **106**, 195301 (2011).
- [9] B. Naylor, E. Marechal, J. Huckans, O. Gorceix, P. Pedri, L. Vernac, and B. Laburthe-Tolra, "Cooling of a Bose-Einstein condensate by spin distillation," (2015), preprint, arXiv:1505.05098.
- [10] R. Olf, F. Fang, G. E. Marti, A. MacRae, and D. M. Stamper-Kurn, Nature Physics **11**, 720 (2015).
- [11] D. M. Stamper-Kurn and M. Ueda, Rev. Mod. Phys. **85**, 1191 (2013).
- [12] X. Li, B. Zhu, X. He, F. Wang, M. Guo, Z.-F. Xu, S. Zhang, and D. Wang, Phys. Rev. Lett. **114**, 255301 (2015).
- [13] A. Mil, T. V. Zache, A. Hegde, A. Xia, R. P. Bhatt, M. K. Oberthaler, P. Hauke, J. Berges, and F. Jendrzejewski, Science **367**, 1128 (2020).
- [14] F. Fang, S. Wu, A. Smull, J. A. Isaacs, Y. Wang, C. H. Greene, and D. M. Stamper-Kurn, Phys. Rev. A **101**, 012703 (2020).
- [15] A. Ramanathan, S. R. Muniz, K. C. Wright, R. P. Anderson, W. D. Phillips, K. Helmerson, and G. K. Campbell, Rev. Sci. Instrum. **83**, 083119 (2012).
- [16] G. E. Marti, A. MacRae, R. Olf, S. Lourette, F. Fang, and D. M. Stamper-Kurn, Phys. Rev. Lett. **113**, 155302 (2014).
- [17] See Supplemental Material at [URL will be inserted by publisher] for further details on spin distribution measurements, the derivation of effective scattering lengths, and of the slight effects of Rb spin-state redistribution on Li spin relaxation.
- [18] This field gradient  $B'_y$  is ramped up at a rate of about 10 G/cm per ms, held at the target value for about 40 ms, and then ramped off before imaging.
- [19] N. Klausen, J. Bohn, and C. Greene, Phys. Rev. A **64**, 053602 (2001).
- [20] This damping is observed by trapping single-element, spin-polarized gases, applying a spin-rotating rf pulse to generate transverse magnetization, waiting a variable time  $\tau$ , and then applying a second spin-rotation rf pulse before measuring the Zeeman-state distribution. Larmor precession during the time  $\tau$  leads to oscillations in the final Zeeman-state distribution, but these oscillations are damped within a few ms. We ascribe this damping to residual magnetic field inhomogeneity, which, in the presence of atomic motion and diffusion, leads to a complete loss of transverse coherence [23].
- [21] This expression for  $\Gamma_\alpha$  is valid so long as the total internal-state energy is the same for the colliding pair before and after the collision. In our experiment, for spin-changing collisions that conserve the total longitudinal spin of the colliding pair, small energy differences arise from the small gyromagnetic ratio difference between  ${}^7\text{Li}$

\* akiraff@berkeley.edu

† Current address: Department of Physics, Universitt Hamburg, 22761 Hamburg, Germany

[1] A. G. Aronov, Jett Lett+ **24**, 32 (1976).

[2] M. Johnson and R. H. Silsbee, Phys. Rev. Lett. **55**, 1790

and  $^{87}\text{Rb}$  and from mean-field energy shifts. However, these energy differences ( $|\Delta E| \lesssim k_B \times 1 \text{ nK}$ ) are far smaller than the thermal energies  $k_B T_{\text{Li}}$  and  $k_B T_{\text{Rb}}$ , and can thus be ignored.

- [22] R. A. W. Maier, M. Eisele, E. Tiemann, and C. Zimmermann, Phys. Rev. Lett. **115**, 043201 (2015).
- [23] J. Higbie, L. Sadler, S. Inouye, A. P. Chikkatur, S. R. Leslie, K. L. Moore, V. Savalli, and D. M. Stamper-Kurn, Phys. Rev. Lett. **95**, 050401 (2005).